Nonequidiffusive premixed-flame propagation in obstructed channels with open, nonreflecting ends

Olatunde Abidakun,[1] Abdulafeez Adebiyi,[1] Damir Valiev,[2] and V'yacheslav Akkerman[1,*]

[1]*Center for Innovation in Gas Research and Utilization (CIGRU), Center for Alternative Fuels, Engines and Emissions (CAFEE), Department of Mechanical and Aerospace Engineering, West Virginia University, Morgantown, West Virginia 26506, USA*

[2]*Center for Combustion Energy, Department of Energy and Power Engineering, Tsinghua University, Beijing 100084, China*

(Received 4 August 2021; accepted 5 January 2022; published 28 January 2022)

Equidiffusive premixed combustion in obstructed channels with both open, nonreflecting ends exhibits various forms of flame propagation: oscillations, acceleration or a combination of both regimes. Given the limited practicality of equidiffusive premixed combustion, it is important to understand how these modes of combustion are altered at nonequidiffusive conditions, characterized by a nonunity Lewis number (thermal to mass diffusivity ratio) Le $\neq 1$. To achieve this, the impacts of Le on the flame dynamics and morphology are analyzed by means of the computational simulations of the reacting flow equations, with Arrhenius chemical kinetics, fully compressible hydrodynamics, and transport properties. In addition to varying Le, the parametric study includes various blockage ratios, channel widths, obstacle spacing and thermal expansion ratios. It is identified how these parameters influence the burning velocities as well as the scaled oscillation amplitude and frequency. Specifically, in the narrow channels with small blockage ratios, the amplitude and frequency of the oscillations vary with Le, with the frequency decreasing and the amplitude increasing as Le grows from 0.3 to 2. In other conditions, a transition from the flame oscillations to sudden flame acceleration or its propagation at a constant velocity is singularly influenced by Le, or by the interplay of Le with the geometric parameters of a channel. The delay time before the onset of flame acceleration, especially at Le < 1, also varies as the channel width and the blockage ratio change. In all cases, Le has both quantitative and qualitative effects on flame propagation in obstructed channels with both open, nonreflecting ends.

DOI: 10.1103/PhysRevE.105.015104

I. INTRODUCTION

Achieving the deflagration-to-detonation transition (DDT) from a weak ignition source, which is often a requirement in many combustion devices such as pulse detonation engines, can be feasible through flame acceleration (FA) [1,2]. On the other hand, moderation of FA to prevent occurrence of DDT in such enclosures as coal mines or underground tunnels is essential for prevention of catastrophic accidents [3–5]. Flame propagation in channels provides a good representation of these combustors and industrial facilities. Depending on a channel geometry, boundary conditions, and the details of flame-wall interaction, a premixed flame can exhibit various modes of propagation, ranging from oscillations to acceleration [6–9]. For instance, in "semi-open" obstructed channels (that with one end closed), FA from the closed end towards the open end is partly due to delayed burning in the pockets between the obstacles [10,11]. More importantly, since there is only one open extreme in a semi-open pipe, the entire burnt gas contributes to pushing the fuel mixture ahead of the flame front, thus resulting in ultrafast acceleration.

In the case of an obstructed channel with both nonreflecting (open) ends, the distribution of the burnt gas between such two ends modifies the flame dynamics, which differs from usual continuous FA encountered in semi-open channels. Flame propagation in such a configuration may proceed in various modes, ranging from oscillations to acceleration, depending on the geometric parameters. Some of the previous works on flame propagation in obstructed channels or tubes with both open, nonreflecting ends include theoretical studies [12], computational simulations [13], and combined experimental and numerical efforts [14]. The measurements [14] reveal that flames in open or vented obstructed conduits accelerate strongly but at a slower rate, as compared to the semi-open pipes [12]. On the other hand, Ref. [13] reported nonlinear quasisteady oscillations of the burning rate, with the oscillation period growing with the blockage ratio but decreasing with the thermal expansion ratio. The authors of Ref. [13] also identified the possibility of FA to replace the oscillations in wider channels. Both experimental and computational results [14] revealed the existence of a slowly propagating flame front, which undergoes instant acceleration without generating shock waves. Pressure oscillations, flame-obstacle interactions, and hydraulic resistance as the cause of sudden FA have been reported.

Another important parameter, with a capability of further disrupting the flame dynamics and morphology, is introduced when burning occurs at nonequidiffusive conditions, that is, unequal diffusion of the mass and heat. This phenomenon is characterized by the Lewis number, Le, which represents the thermal-to-mass diffusivity ratio, with Le $= 1$ for equidiffusive and Le $\neq 1$ for nonequidiffusive conditions. The impact of Le $\neq 1$ on the flames propagating in semi-open channels or

*Corresponding author: Vyacheslav.Akkerman@mail.wvu.edu

tubes ranges from promotion to moderation of FA, as it alters the internal flame structure, and thereby, the flame response to curvature and stretch [15–19]. Specifically, the Le < 1 condition introduces the diffusional-thermal instability into the overall dynamics and leads to the interplay between the internal and global flame structures. On the other hand, the Le > 1 condition results in a thickening of the flame front, a decrease in the local burning temperature and, hence, moderation of FA [17–19]. The impact of Le has also been found to be substantial for the flames propagating in the presence of turbulence [20].

Therefore, the question is what the impact of Le would be on the dynamics and morphology of oscillating and accelerating flames in channels with open, nonreflecting ends. To answer this question, we have performed a computational study of the effects of Le on premixed laminar flame dynamics. Recently, we have addressed this problem in unobstructed channels [21], while in the present work we deal with obstructed channels. Specifically, flame propagating through a comb-shaped array of obstacles in two-dimensional (2D) channels with both open, nonreflecting ends is studied by means of computational simulations of the reacting flow equations, with fully compressible hydrodynamics and Arrhenius chemistry. In addition to considering various Le, the parametric study involves the variations of the blockage ratio, channel width, and obstacle spacing. The flames are found to exhibit both the oscillations and acceleration as the burning conditions vary, with the changes in Le and its interplay with other parameters being the cause of an oscillation-to-acceleration transition.

II. DESCRIPTION OF THE COMPUTATION SIMULATIONS

We have performed computational simulations of the hydrodynamic and combustion equations including transport processes (viscosity, diffusion, and heat conduction) and chemical kinetics modelled by a one-step Arrhenius reaction. The basic equations in a 2D geometry take the form

$$\frac{\partial}{\partial t}\rho + \frac{\partial}{\partial x_i}(\rho u_i) = 0, \tag{1}$$

$$\frac{\partial}{\partial t}(\rho u_i) + \frac{\partial}{\partial x_j}(\rho u_i u_j + \delta_{ij}P - \gamma_{i,j}) = 0, \tag{2}$$

$$\frac{\partial}{\partial t}\left(\rho e + \frac{1}{2}\rho u_i u_j\right) + \frac{\partial}{\partial x_i}\left(\rho u_i h + \frac{1}{2}\rho u_i u_j u_j + q_i - u_j \gamma_{i,j}\right) = 0, \tag{3}$$

$$\frac{\partial}{\partial t}(\rho Y) + \frac{\partial}{\partial x_i}\left(\rho u_i Y - \frac{\zeta}{S_c}\frac{\partial Y}{\partial x_i}\right) = -\frac{\rho Y}{\tau_R}\exp\left(-E_a/R_p T\right), \tag{4}$$

where Y is the mass fraction of the fuel mixture, $e = QY + C_v T$ and $h = QY + C_P T$ are the specific internal energy and enthalpy, respectively; $Q = C_P T_f(\Theta - 1)$ is the energy release in the reaction, and C_v, C_P are the specific heats at constant volume and pressure, respectively. Both the unburned and burnt matters are assumed to be two-atomic ideal gases of the same constant molecular weight, $m = 2.9 \times 10^{-2}$ kg/mol, with $C_v = 5R_p/2m$, $C_p = 7R_p/2m$, such that the adiabatic

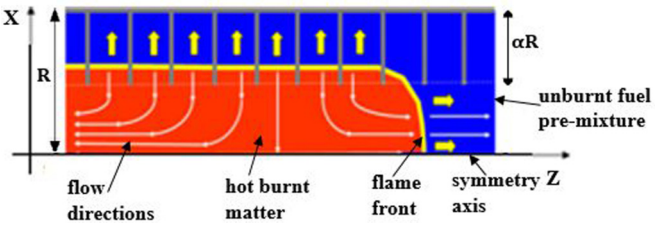

FIG. 1. An illustration of flame propagation in an obstructed channel with both extremes open (only an upper half is shown).

index is $k \equiv C_p/C_v = 1.4$. Here $R_p = 8.314$ J/(mol K) is the universal gas constant, and the equation of state is

$$P = \rho R_p T/m. \tag{5}$$

The initial fuel density, pressure, and temperature are $\rho_f = 1.16\text{kg/m}^3$, $P_f = 100$ kPa, and $T_f = 300$ K, respectively. The stress tensor $\gamma_{i,j}$ and the energy diffusion vector q_i are given by

$$\gamma_{i,j} = \zeta\left(\frac{\partial u_i}{\partial x_j} + \frac{\partial u_j}{\partial x_i} - \frac{2}{3}\frac{\partial u_k}{\partial x_k}\delta_{i,j}\right),$$
$$q_i = -\zeta\left(\frac{C_p}{\text{Pr}}\frac{\partial T}{\partial x_i} + \frac{Q}{\text{Sc}}\frac{\partial Y}{\partial x_i}\right), \tag{6}$$

where $\zeta = \rho\nu$ is the dynamic viscosity having a value of 1.7×10^{-5}kg/(m s) in the fuel mixture, Pr and Sc are the Prandtl and Schmidt numbers, respectively. The Lewis number is calculated as their ratio, Le $=$ Sc/Pr. In this work, Le is varied in the range $0.3 \leqslant \text{Le} \leqslant 2.0$, by keeping the Prandtl number constant, Pr $= 1$, and adjusting the Schmidt number, Sc, accordingly. The right-hand side of Eq. (4) describes an irreversible one-step Arrhenius reaction of the first order, with the activation energy $E_a = 79.82$ kJ/mol and the constant of time dimension $\tau_R = 4.06 \times 10^{-10}$ s. A conventional unit of velocity dimension is the unstretched laminar flame velocity S_L. In the present work, $S_L = 34.7$ cm/s, being 10^3 times smaller than the initial speed of sound in this fuel mixture, $c_0 = 347$ m/s, such that the hydrodynamics is almost incompressible at the initial stage of burning. A useful unit of length dimension is the thermal flame thickness, which is defined, conventionally, as $L_f \equiv \zeta_f/\rho_f S_L \text{Pr} = 4.22 \times 10^{-5}$ m. We, therefore, measure the half-width of the channel R in terms of L_f.

In this work, we consider a premixed-flame front propagating in a long 2D channel of width $2R$, with a blockage ratio α, such that a fraction of the channel of width $2R\alpha$ is occupied by equally and tightly spaced obstacles as illustrated in Fig. 1. The spacing between the adjacent obstacles is taken to be $\Delta Z = R/4$, in most cases, but the cases of $\Delta Z = R/2$ and R are also considered, with the channel half-widths $R/L_f = 12, 24, 36$, the blockage ratios $\alpha = 1/3, 1/2, 2/3$, and the thermal expansion ratios $\Theta = 5, 8, 12$. The quantities Θ and E_a determine the Zeldovich number Ze,

$$\text{Ze} = \frac{E_a}{R_p T_f}\frac{(\Theta - 1)}{\Theta^2}, \tag{7}$$

such that in the present work we have Ze $= 5.12, 3.50$, and 2.44 for $\Theta = 5, 8$, and 12, respectively. The channel

length was up to 150 R, thereby making the aspect ratio up to 75. It is nevertheless noted that as long as the flows remain substantially subsonic, the flow effects that drive the flame dynamics are more local, whereas hydraulic resistance, and thereby, the whole channel length are much less important as we demonstrated and discussed earlier in [8]. However, the channel length and hydraulic resistance eventually become important with an increase in the flame propagation Mach number; see, for instance, Refs. [12,14] for more details on the subject.

The flame response to various parameters is monitored by the instantaneous burning rate [22],

$$U_w = \frac{1}{2R\rho_f}\int \frac{\rho Y}{\tau_R}\exp\left(-\frac{E_a}{R_p T}\right)dx\,dz. \tag{8}$$

A convenient measure of the instantaneous flow compressibility and, thereby, the stage of DDT is the instantaneous Mach number associated with the flame tip, $\mathrm{Ma}_{\mathrm{tip}}(t) = U_{\mathrm{tip}}/c_{\mathrm{tip}}$, where $U_{\mathrm{tip}} \equiv dZ_{\mathrm{tip}}/dt$ is the flame tip velocity in the laboratory reference frame and $\mathrm{c}_{\mathrm{tip}}$ is an instantaneous sound speed taken at the flame tip,

$$\mathrm{c}_{\mathrm{tip}} \equiv \sqrt{\left(\frac{C_p}{C_v}\right)\left(\frac{R_p}{m}\right)T_{\mathrm{tip}}}. \tag{9}$$

The surfaces of the channel walls and obstacles are adiabatic, $\mathbf{n}\cdot\nabla T = 0$, and free-slip, $\mathbf{n}\cdot\mathbf{u} = 0$, where $\mathbf{n}$ is a normal vector at a surface. The nonreflecting boundary conditions are employed at both extremes of the channel to prevent the reflection of the sound waves and weak shocks. The initial flame structure is imitated by the Zeldovich-Frank-Kamenetsky (ZFK)-like solution for a planar flame front initiated at a distance of 60 L_f from the left extreme of the channel.

Similar to our previous works [13,17–19], the numerical approach is based on a cell-centered, finite-volume numerical scheme, which is of the second order of approximation in time and of the fourth order of approximation in space for convective terms, and it is of the second order of approximation in space for diffusive terms. The computational platform employs the conservation Eqs. (1)–(4) in a unified form:

$$\frac{\partial G}{\partial t} + \frac{\partial E_G}{\partial z} + \frac{\partial F_G}{\partial x} = H_G, \tag{10}$$

where G stands for any of the variables ρ, ρu_x, ρu_z, ρu_x, ρY, ε; the functions E_G and F_G are the related axial and radial fluxes, respectively, and H_G is the source term. The spatial discretization is obtained by integrating any of the conservation laws (1)–(4) in the form (10) over a given grid cell.

To reduce the computational time and memory, similar to our previous computational works [13,17–19], a self-adaptive structured grid is used: namely, it is rebuilt based on the positions of the flame front and the leading pressure wave. This is achieved by using the third-order splines to interpolate the flow variables during the grid reconstruction, preserving the second order of approximation of the numerical scheme. Specifically, the numerical mesh is rectangular, with the cell sides being parallel to the radial and axial directions. While the radial grid size is fixed, ΔZ_f, the axial grid size changes dynamically, from the minimal value of ΔZ_f to the maximal value of ΔZ (spacing between the obstacles), keeping the finer resolution at the flame front and at the pressure wave generated by the flame motion. Similar to our previous works [13,17], here we employed $\Delta Z_f = 0.2\ L_f$ as validated by the grid resolution test presented in the Appendix, which is performed in a manner similar to our previous works on obstructed channels [13,17]. Obviously, the usage of such adaptive mesh notably reduces the computational resources required for this work. For example, if only a fine square grid $0.2\ L_f \times 0.2\ L_f$ was used, then our computational domain would contain up to $150 \times 2 \times 36^2 \times 5^2 \sim 9.7$ million cells, while in practice it never exceeded 1–2 million cells.

III. RESULTS AND DISCUSSION

A. Morphology and dynamics of nonequidiffusive flames in channels with nonreflecting ends

The color temperature snapshots in Fig. 2 show the morphology of the nonequidiffusive flame fronts of $\mathrm{Le} = 0.3$ [Fig. 2(a)] and $\mathrm{Le} = 2$ [Fig. 2(b)] as they propagate through an obstructed channel with both open, nonreflecting ends. Here the temperature changes from 300 K (blue) in the fresh fuel mixture to 2400 K (red) in the burnt matter such that the thermal expansion ratio is $\Theta = 8$. The white lines with the arrows represent the streamlines of the flow. The concentrated "white areas" (spots) are devoted to the sporadic vortices stored in the pockets between the obstacles. We have observed similar structures earlier, for instance, in Ref. [1].

In both cases considered in Fig. 2, $\mathrm{Le} = 0.3$ and $\mathrm{Le} = 2$, the initial internal flame structure is approximated by the ZFK-like solution, Fig. 2(a)(i), and it results in a corrugated shape of the flame front, with the extent of the curvature determined by the burning conditions. Variations in the flame shape are largely dependent on the response of the flame to the curvature caused by the rearward flow of the premixture ahead of the flame front. The temperature snapshots for $\mathrm{Le} = 0.3$ differ from those for $\mathrm{Le} = 2$, necessitated by the need to cover the full extent of the shape changes encountered in each case. In the case of $\mathrm{Le} = 0.3$, Fig. 2(a), an initially planar flame front quickly acquires a concave shape at the center of the channel and a convex shape towards the obstructed sides, resulting in an increased flame surface area. We also see a wider preheated zone at the center of the channel in Fig. 2(a)(ii). As the preheated fuel mixture is consumed, the cusp previously formed at the center of the channel decreases, Fig. 2(a)(iii), causing FA and a reduction in concavity of the flame front. This acceleration lasts shortly as the distributed nature of the flow prevents the burnt gas from providing adequate push on the fuel mixture, causing the flame front to revert to a shape with a concave center and a wide preheated zone, described earlier. The back and forth push from the burnt gas and the fuel mixture continues, culminating in the oscillations of the flame propagating through the channel. For $\mathrm{Le} = 2$, Fig. 2(b), it takes more time for the flame front to acquire an appreciable concave shape with a thinner preheated zone at the center, Fig. 2(b)(ii). The flame front keeps being corrugated, almost forming a tulip shape, Fig. 2(b)(iii), before the fuel mixture is consumed and FA occurs. The process is repeated, causing periodic flame oscillations. However, the oscillations, in this

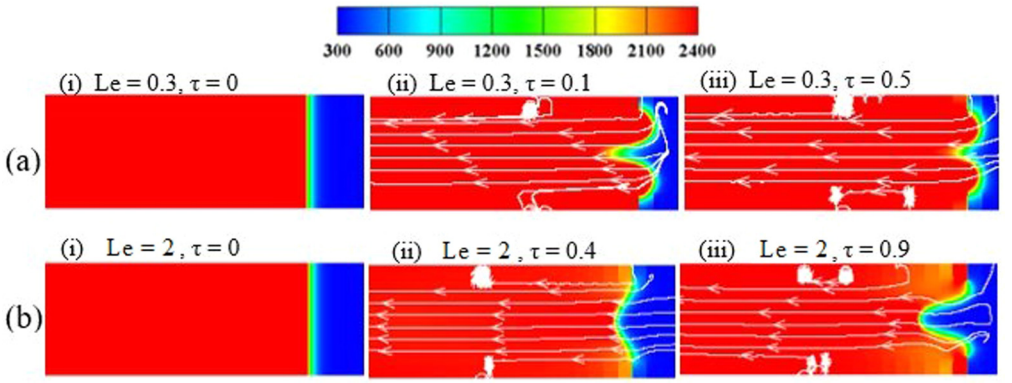

FIG. 2. The typical temperature snapshots for the evolution of a flame with $\Theta = 8$ during one oscillation in a channel with $R = 12L_f$, $\alpha = 1/3$ for Le $= 0.3$ (a) and Le $= 2$ (b). The white lines with the arrows represent the streamlines of the flow.

case, are expected to have a higher period, as it takes longer for a flame front to respond to a distortion caused by the rearward flow of the fuel mixture.

A further illustration of the effect of Le on flame propagation is done by plotting the scaled total burning rate vs the scaled time for various operating conditions. Additional characterization is done by examining the physical appearance of the waveform, estimating the average oscillation frequency and amplitude. These plots provide a further illustration of how the flame dynamics is affected by the Lewis number. Figure 3(a) shows the scaled total burning rate vs the scaled time for the channel of half-width $R = 12L_f$, the blockage ratio of $\alpha = 1/3$, and the thermal expansion ratio of $\Theta = 8$, with each subplot pallet representing a different Le, for clarity. For all the Lewis numbers considered, the flames oscillate as they go through a narrow channel. Such oscillations, however, exhibit varying quality in terms of the oscillation frequency and amplitude.

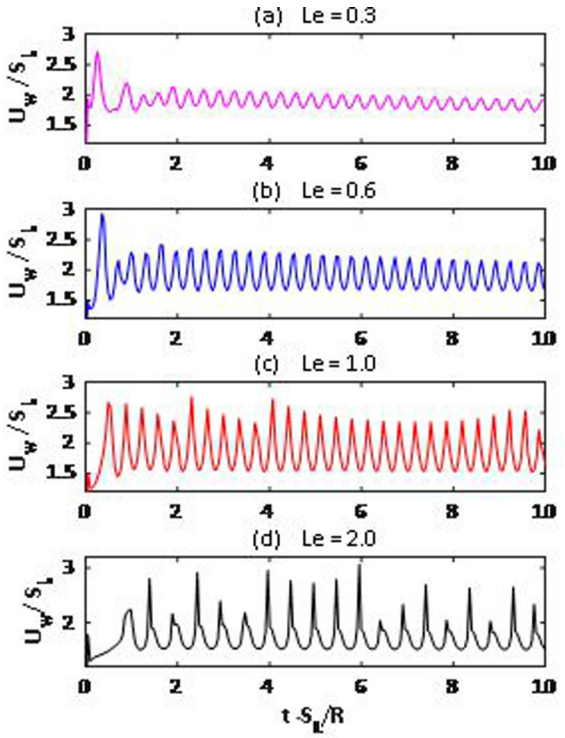

FIG. 3. The scaled burning rate U_w/S_L vs the scaled time tS_L/R for the thermal expansion ratio $\Theta = 8$, the blockage ratio $\alpha = 1/3$, the obstacle spacing $\Delta Z = R/4$, the channel width $R = 12\ L_f$, and various Lewis numbers Le $= 0.3$ (a), 0.6 (b), 1 (c), and 2 (d).

Figure 4 presents the scaled oscillation amplitude, $\Delta U_w/S_L$, and frequency, f_p (scaled by S_L/R), vs Le for $\Theta = 8$, $R = 12\ L_f$, $\alpha = 1/3$, and $\Delta Z = R/4$. Here the amplitudes were calculated using the maximal and minimal scaled burning rates in Fig. 3, $\Delta U = (U_{w,\max} - U_{w,\min})/2$, while the frequencies were determined as the number of complete oscillations per period from the same plot. According to Fig. 4, the flame oscillation amplitude increases when the Lewis number grows from Le $= 0.3$ to 1, while it declines when Le grows further, to Le $= 2$. There is no noticeable difference in the oscillation frequency when Le is increased from Le $= 0.3$ to 0.6; however, the further increase in the Lewis number, to

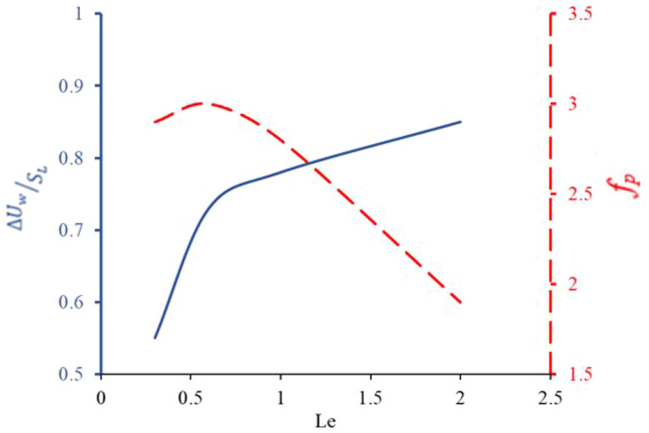

FIG. 4. The scaled oscillation amplitude, $\Delta U_w/S_L$, and frequency, f_p (scaled by S_L/R), vs the Lewis number, Le, for the thermal expansion ratio $\Theta = 8$, the channel half-width $R = 12\ L_f$, the blockage ratio $\alpha = 1/3$, and the obstacle spacing $\Delta Z = R/4$. The amplitudes were calculated using the maximal and minimal values of the scaled burning rates in Fig. 3, $\Delta U = (U_{w,\max} - U_{w,\min})/2$, while the frequencies were determined as the number of complete oscillations per period from the same plot.

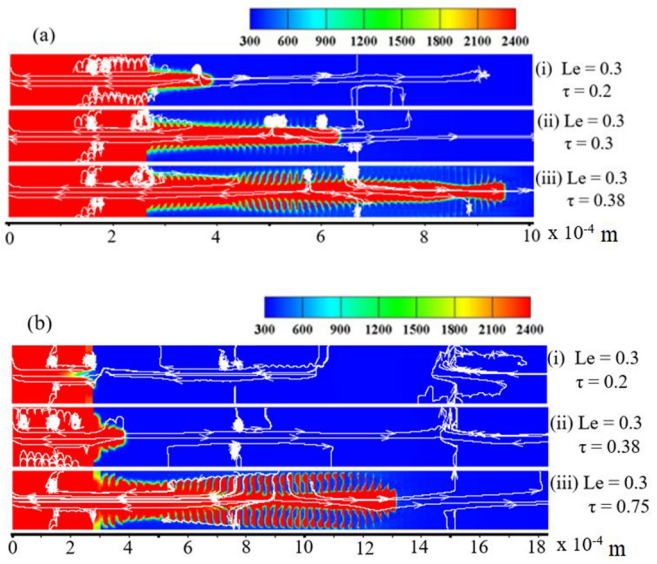

FIG. 5. The color temperature snapshots for the evolution of a flame with Le = 0.3, $\Theta = 8$, in a channel with $\alpha = 2/3$ and $R = 12L_f$ (a) and $R = 24L_f$ (b). The white lines with the arrows represent the streamlines of the flow.

Le = 2, results in the reduction of the oscillation frequency f_p (scaled by S_L/R) from 3 to 1.9. For equidiffusive flames, Le = 1, such an oscillatory behavior can be attributed to the hydraulic resistance of the flow ahead of the flame front and the distributed flow of the burnt gas in a channel with open, nonreflecting ends. While the distributed flow is still encountered in the nonequididffusive burning conditions, additional contributions to the flame dynamics from nonequidiffusivity can be caused by the internal flame structure. Specifically, a thinner flame front and a high local burning temperature, intrinsic to the events of Le < 1, result in a faster response to the flame stretch caused by the backward flow of the unburnt mixture, and, thus, the lower amplitude and the higher frequency of the flame oscillations are observed. On the other hand, a thicker flame front at the condition of Le $\geqslant 1$ is able to withstand the higher stretch from the backward flowing premixtures, causing the delayed responses and, consequently, the lower oscillation frequencies and the higher oscillation amplitudes as compared to the Le < 1 case.

The color temperature snapshots for the $\Theta = 8$, Le = 0.3 flame, propagating through the channels with a blockage ratio of $\alpha = 2/3$ and the channel half-widths of $R = 12\ L_f$ and $24\ L_f$, shown in Figs. 5(a) and 5(b), respectively, exhibit a propagation mode different from the oscillatory mode observed earlier. In both cases of half-widths $12\ L_f$ and $24\ L_f$, the flames accelerate as they propagate through the channel. For $R = 12L_f$, the initial ZFK-like planar flame front swiftly acquires a prolonged convex shape, Fig. 5(a)(i), signifying an increased flame surface area and, thus, FA. Flame propagation, however, occurs only in the central, unobstructed segment of the channel, with the fuel mixture in the side pockets left unburnt, Fig. 5(a)(ii). While consumption of the fuel mixture in the side pocket is delayed at the initial stage, lateral propagation is observed to increase as the flame front moves on from its ignition position, Fig. 5(a)(iii). This poses the possibility of a thermal explosion, as the contribution of delayed burning in the cutoff region to the propagating front will be immense when it finally occurs. An increase in the channel half-width to $R = 24\ L_f$ results in slightly delayed FA, with the flame channeling occurring right after ignition; see Fig. 5(b)(i). The flame front changes to acquire a convex shape, propagating into the side pockets [Fig. 5(b)(ii)]. Due to the increased flame surface area, such a flame accelerates with more lateral propagation away from the ignition position [Fig. 5(b)(iii)].

Various regimes of flame propagation are clearly seen in the plots of Fig. 6(a) showing the evolution of the burning rate. In the case of Le = 0.3, the flame shows slight initial quasisteady propagation, and then transition to an accelerating regime, with acceleration being quite strong [the respective scaled total burning rate is represented on the left vertical axis of Fig. 6(a)]. Strong and sudden FA observed here is similar to that reported and discussed in Ref. [12]. This is followed by slight deceleration before another round of quasisteady oscillations around the flame saturation velocity. Despite the effect of distributed flow, which is known to limit FA in channels with both nonreflecting ends, it is interesting to see that the combined effects of the low Le and high α (such as $\alpha = 2/3$) can produce enough momentum to overcome the hydraulic resistance, and eventually transit to acceleration. In the cases of Le = 0.6 and 1, the flame spreads oscillating around a steady velocity, with the oscillation frequency being much lower at Le = 1. On the other hand, at Le = 2, the burning rate plot shows that the flame propagates through the channel at a constant velocity. This indicates a balance between the push effect of the burnt gas and the resisting force. The burning rate for Le = 0.6, 1, and 2 is represented by the right vertical axis in Fig. 6(a). The plot for the evolution of the burning rate in the case of $\Theta = 8$, $\alpha = 2/3$, $\Delta Z = R/4$, and $R = 24\ L_f$ in Fig. 6(b) shows that the flames exhibit sudden acceleration at the Lewis numbers of Le = 0.3, 0.6, 1. These flames, however, undergo near-steady initial propagation before the onset of FA. The time of such initial propagation increases as the Lewis number grows from Le = 0.3 to 0.6. A similar behavior is also seen for the Le = 1 flame, while neither oscillations nor acceleration are observed for the Le = 2 flames. Also, the maximum burning rate, attained by a flame before propagation at a saturation velocity, is lower for Le = 0.3 as compared to the cases of Le = 0.6 and 1. However, the saturation velocity falls within the same range for all three cases.

Establishing the occurrence of the flame transitioning between the oscillating and acceleration regimes under the impact of Le provides a fascinating result: as Fig. 6 indicates, the Lewis number provides both qualitative and quantitative effects on the flame dynamics in the channels with open, nonreflecting ends. Another interesting phenomenon, observed in the results presented above, is the existence of interrelations between the Lewis number and the geometric parameters of the channel, such as the channel width and the blockage ratio. For a clearer understanding of these couplings, the Le-α and Le-R interrelations are separately presented and discussed below.

In a semi-open channel, with a flame ignited at the closed end and travelling towards the open end, each of Le and α have been individually reported to influence FA. In particular, this

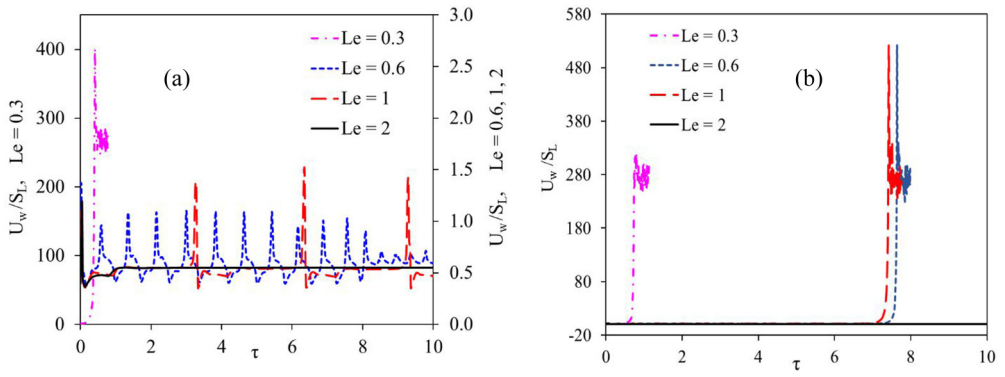

FIG. 6. The scaled burning rate U_w/S_L vs the scaled time $\tau = tS_L/R$ for the $\Theta = 8$ flames at various Lewis numbers Le = 0.3, 0.6, 1, 2, propagating in the channels with the blockage ratio $\alpha = 2/3$, the obstacle spacing $\Delta Z = R/4$, at various channel half-widths: $R = 12\ L_f$ (a) and $R = 24\ L_f$ (b).

is because of the changes in the flame thickness or the changes in the local burning temperature, due to the Le variations [17,18], and also because of the impact of delayed burning inside the pockets on the flame as the blockage ratio α varies [10]. The impact of Le on flame propagation, as seen here, is either enhanced or suppressed by α.

Figure 7 presents the time evolution of the scaled burning rate for $\Theta = 8$, $\Delta Z = R/4$, and $R = 24\ L_f$. Here, for Le = 0.3 [Fig. 7(a)], the flames accelerate for all three blockage ratios considered. However, the transition to acceleration occurs faster as the blockage ratio increases from $\alpha = 1/3$ to $\alpha = 2/3$. The maximum burning rate attained and the saturation velocity also differ for these three cases. The trend of a decreasing initial flame propagation period with the blockage ratio, observed here, is similar to the trend of an increasing acceleration rate observed for various α in a semi-open channel. Specifically, a higher α is found to provide faster acceleration in the Bychkov mechanism [10,23], when other conditions are fixed, because of a larger volume of the burnt gas being released into the central unobstructed part of the channel after delayed burning in the side pockets. Such a decrease in the initial propagation time at Le = 0.3 as α increases can be attributed to a coupling of this delayed burning to other attributes of a low-Le flame—such as a thinner flame front, a higher local heating temperature, and a faster response to the flame stretch—all of which enhance FA. On the other hand, no FA is observed for all the blockage ratios considered when Le = 2 [Fig. 7(b)]. Namely, the flame is seen to oscillate at $\alpha = 1/3$ and $1/2$, while it only propagates at constant velocity if the blockage ratio is higher, such as $\alpha = 2/3$. In this case, an increase in the blockage ratio to $2/3$ results in the suppression of the oscillations observed at the lower blockage ratios. The interplay between a higher volume of the gas produced from delayed burning in the side pockets and other conditions, provided by a high Lewis number, which is known to moderate FA, is only enough to balance the resisting force, therefore, resulting in steady flame propagation.

Also, an interplay between Le and R is explored in Fig. 8 by showing the scaled burning rate vs the scaled time for $\Theta = 8$, $\alpha = 2/3$, and Le = 0.3 and 2. All the three propagation regimes (namely, that of initial propagation at a constant velocity, that of sudden acceleration, and that of the oscillations around a saturation velocity) are exhibited by the flames when Le = 0.3 [Fig. 8(a)] for R ranging from $12\ L_f$ to $48\ L_f$. The acceleration rates, the maximum scaled burning rates, and the saturation velocities fall within the same range for

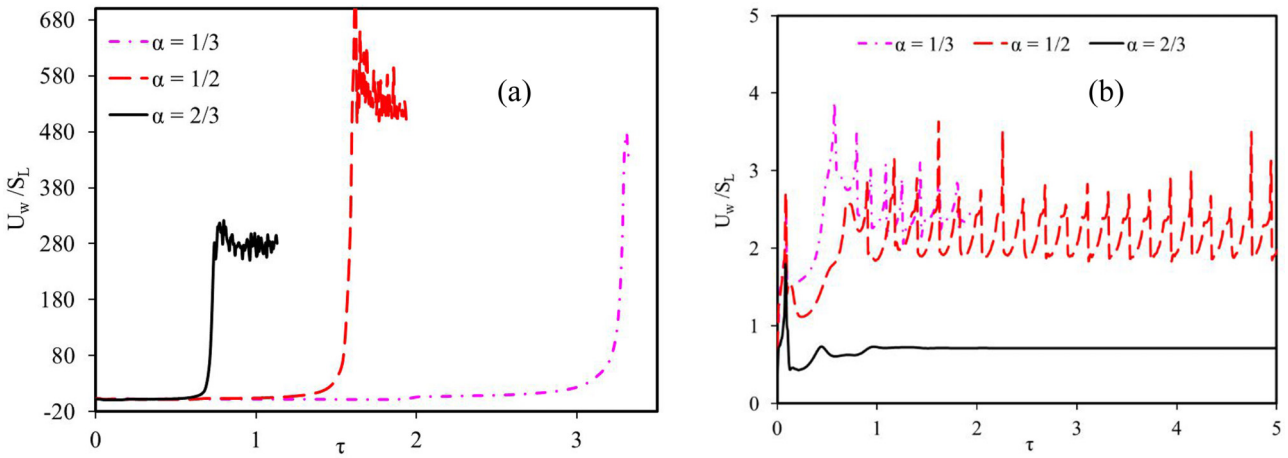

FIG. 7. The scaled total burning rate U_w/S_L vs the scaled time tS_L/R for the thermal expansion ratio $\Theta = 8$, the obstacle spacing $\Delta Z = R/4$, the channel half-width $R = 24\ L_f$, various blockage ratios $\alpha = 1/3, 1/2, 2/3$, at various Lewis numbers Le = 0.3 (a) and Le = 2 (b).

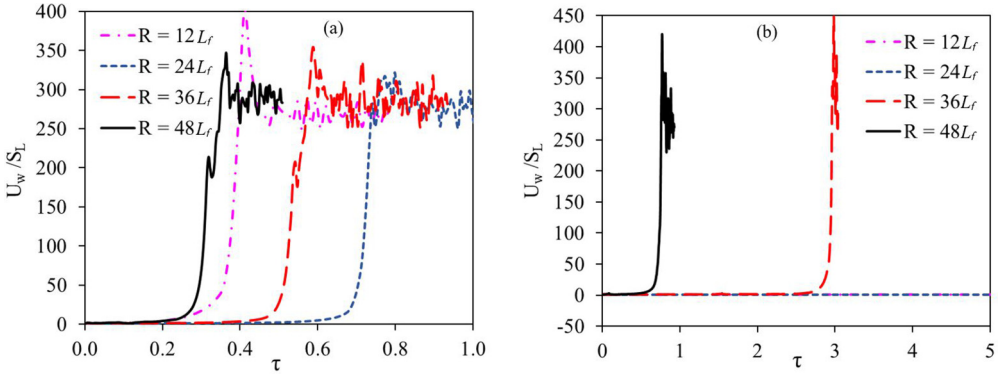

FIG. 8. The scaled total burning rate U_w/S_L vs the scaled time tS_L/R for the thermal expansion ratio $\Theta = 8$, the obstacle spacing $\Delta Z = R/4$, the blockage ratio $\alpha = 2/3$, for the channels of half-widths $R = 12\ L_f, 24\ L_f,\ 36\ L_f,\ 48\ L_f$, at various Lewis numbers Le = 0.3 (a) and Le = 2 (b).

all the channel widths considered. This supports the Reynolds independence of the original Bychkov mechanism of FA [10]. However, an interesting situation is seen in the delay time prior to acceleration, i.e. the time taken for the initial propagation.

The observed increase in the delay time when R increases from 12 L_f to 24 L_f is reversed by increasing R to 36 L_f, with the delay time decreasing further by increasing R to 48 L_f. This delay prior to acceleration was, however, attributed to the effect of hydraulic resistance (viscous effect) in Ref. [12], with the delay time stated to reduce to zero as $R/L_f \to \infty$. This assertion, however, does not hold under some conditions in this case: for $R = 12\ L_f$ to 24 L_f. The reversal, experienced between $R = 24\ L_f$ and $R = 36\ L_f$, indicates the presence of a threshold within this region, which might depend on the ratio of the flame thickness to the channel half-width or some other effects. At Le = 2 [Fig. 8(b)], acceleration is observed only for $R = 36\ L_f$ and $R = 48\ L_f$, with the delay time prior to the onset of acceleration decreasing as R grows from 36 L_f and 48 L_f. In narrower channels (such as $R = 12\ L_f$ and $R = 24\ L_f$), the flames propagated with a constant velocity.

Increasing the spacing between the obstacles from $\Delta Z = R/4$ to $\Delta Z = R/2$ and $\Delta Z = R$ (most especially, for the cases of Le < 1, where the existence of different modes of flame propagation has been established) shows that the delay time prior to acceleration is also impacted. Figure 9(a) shows the scaled burning rate vs the scaled time for Le = 0.3, $\Theta = 8$, $R = 24L_f$, and $\alpha = 1/2$, with the delay time before transition to sudden acceleration decreasing as the obstacle spacing is increased from $R/4$ to $R/2$. The delay time, however, grows when the obstacle spacing is increased to R. While flame propagation is not affected, qualitatively, as the obstacle spacing varies, the changes observed in the delay time might be due to the competing contributions of delayed burning in the pockets and vorticity. According to the Bychkov mechanism of FA in obstructed conduits [10], a role played by turbulence, though supplementary, is nevertheless known to grow with an increase in the spacing between the obstacles [7,23] and, thus, turbulence is expected to contribute to the shortening of the delay time. However, the time, required before a contribution of delayed burning is experienced in the unobstructed segment of the channel, also grows with the obstacle spacing, due to an increased volume of the fuel mixture per pocket. When the blockage ratio is increased to $\alpha = 2/3$ [Fig. 9(b)], for the reason similar to that discussed for a channel with $\alpha = 1/2$, the delay time grows by increasing the obstacle spacing ΔZ

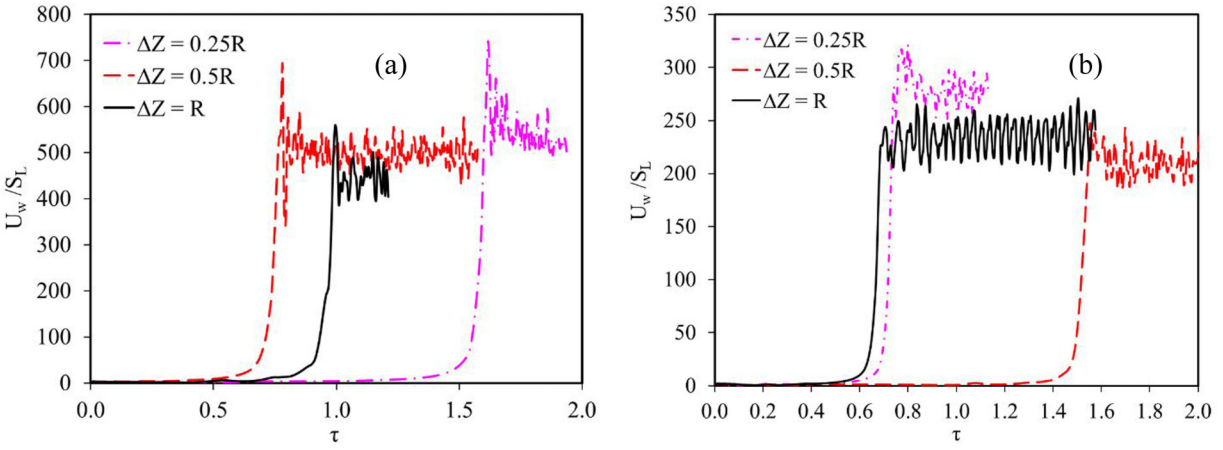

FIG. 9. The scaled total burning rate U_w/S_L vs the scaled time tS_L/R for the thermal expansion ratio $\Theta = 8$, the channel half-width $R = 24\ L_f$, the Lewis number Le = 0.3, for various obstacle spacing $\Delta Z = R/4, R/2, R$, and various blockage ratios $\alpha = 1/2$ (a) and 2/3 (b).

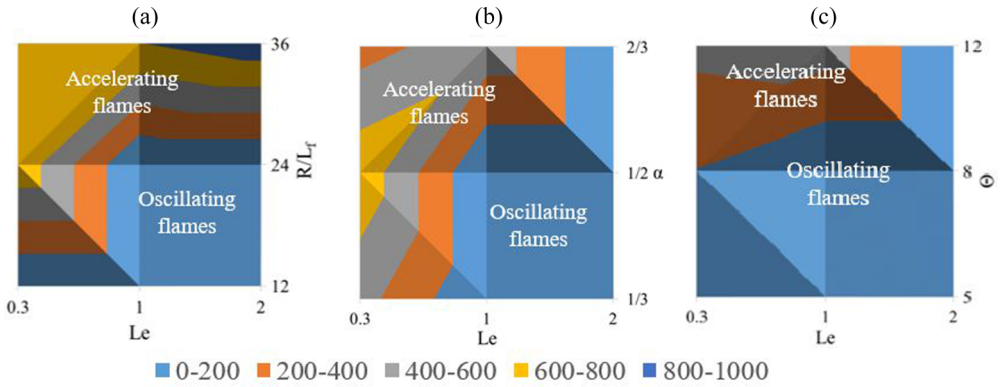

FIG. 10. Oscillating and accelerating regimes of flame propagation: R-Le diagram at $\alpha = 1/2$, $\Delta Z = R/4$, and $\Theta = 8$ (a); α-Le diagram at $R = 24L_f$, $\Delta Z = R/4$, and $\Theta = 8$ (b); and Θ-Le diagram at $R = 24L_f$, $\Delta Z = R/4$, and $\alpha = 1/3$ (c). Colors represent the scaled burning rate U_w/S_L.

from $R/4$ to $R/2$, but it decreases for larger ΔZ. However, the higher blockage ratio, $\alpha = 2/3$, alters the flame dynamics, and consequently, the time taken before transition to acceleration.

Finally, the contour maps of Fig. 10, where the colors represent the scaled burning rate U_w/S_L, demonstrate the regimes of flame propagation, namely, the oscillations and acceleration, exhibited by the propagating flame front under different geometrical and thermo-chemical conditions. It is seen from Fig. 10(a) that the tendency of the flame to accelerate grows with the channel width, for all Le considered. However, the critical width at which acceleration occurs is lower for the Le $= 0.3$ flame as compared to the Le $\geqslant 1$ flames. The map of the blockage ratio α vs the Lewis number Le at $R = 24L_f$, $\Delta Z = R/4$, and $\Theta = 8$ [Fig. 10(b)] indicates that the Le $= 2$ flames oscillate, and the Le $= 0.3$ flames accelerate for all the blockage ratios considered. Variation of the thermal expansion ratio Θ at various Le and fixed $R = 24R_f$, $\Delta Z = R/4$, and $\alpha = 1/3$, in Fig. 10(c), shows that an increase in Θ from $\Theta = 5$ to $\Theta = 12$ only causes a Le $\leqslant 1$ flame to accelerate. The impact of higher thermal expansion is not enough to cause acceleration in the case of Le $= 2$. In all cases, it is observed that the tendency of the flame to accelerate increases as Le decreases.

B. Oscillation-to-acceleration transition mechanism for low-Le flames

The flame evolution leading to sudden acceleration, discussed above, is illustrated by the color temperature snapshots of Fig. 11. Specifically, at the scaled time $\tau = tS_L/R = 0.4$, Fig. 11(i), the hot spots and the flame segments, not connected to the major propagating flame segment, are observed to be formed between the obstacles. Spontaneous combustion caused by this condition results in a thermal explosion and the formation of additional hotspots, as seen in Fig. 11(ii). The interplay of the thermal explosion resulting from this spontaneous combustion, and the eventual completion of delayed burning occurring upstream in the channel, Fig. 11(iii), provides an enough force to create sudden acceleration. Compression of the fuel mixture ahead of the propagating flame results in the increased pressure and temperature in the fuel mixture, which can cause formation of the hot spots.

Figure 12 presents the scaled burning rate, U_w/S_L, Fig. 12(a), the temperature at the fuel side of the flame tip, T_{tip}, Fig. 12(b), as well as the instantaneous Mach number at the flame tip, $\text{Ma}_{\text{tip}} = U_{\text{tip}}/c_{\text{tip}}$, Fig. 12(c), vs the scaled time $\tau = (S_L t)/R$. Here, the lines of similar color and type represent the same half-width R in all three subfigures. These plots reveal that the three parameters, Ma_{tip}, U_w/S_L, and T_{tip}, follow the same trend. However, it is observed that Ma_{tip} starts growing first, before U_w/S_L and T_{tip} do. At the early stage, when Ma_{tip} is low, both the flame temperature and the scaled burning rate also maintain low values. However, both T_{tip} and U_w/S_L grow swiftly, signifying a transition to sudden acceleration, when a threshold value of the flame tip Mach number is attained, being in the range $1 \leqslant \text{Ma}_{\text{tip}} \leqslant 2$ for the channel half-widths $R = 12\ L_f, 24\ L_f, 36\ L_f$. In this light, sudden FA can be devoted to compressibility in a channel as the compression of the fuel mixture ahead of the flame results in the increased temperature and, consequently, the increased burning rate. However, while compressibility has previously been found to moderate FA in obstructed semi-open channels [24], in the present configuration it is found to be responsible for sudden FA.

The solid horizontal lines in Figs. 12(a)–12(c) designate the Chapman-Jouguet (CJ) detonation Mach number [25]

$$\text{Ma}_{CJ} = \sqrt{1 + \frac{1}{2}(k+1)(\Theta - 1)} + \sqrt{\frac{1}{2}(k+1)(\Theta - 1)}. \tag{11}$$

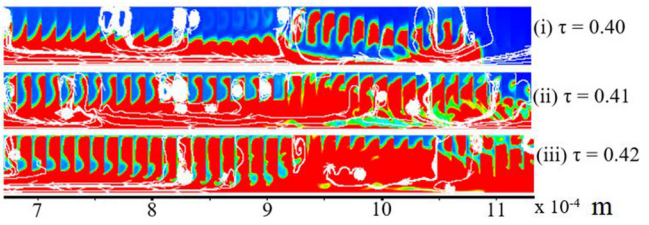

FIG. 11. The color temperature snapshots for the evolution of a flame with $\Theta = 8$, Le $= 0.3$ propagating in a channel with $\alpha = 2/3$, $R = 12\ L_f$ (a partial section view). The white lines with the arrows represent the streamlines of the flow.

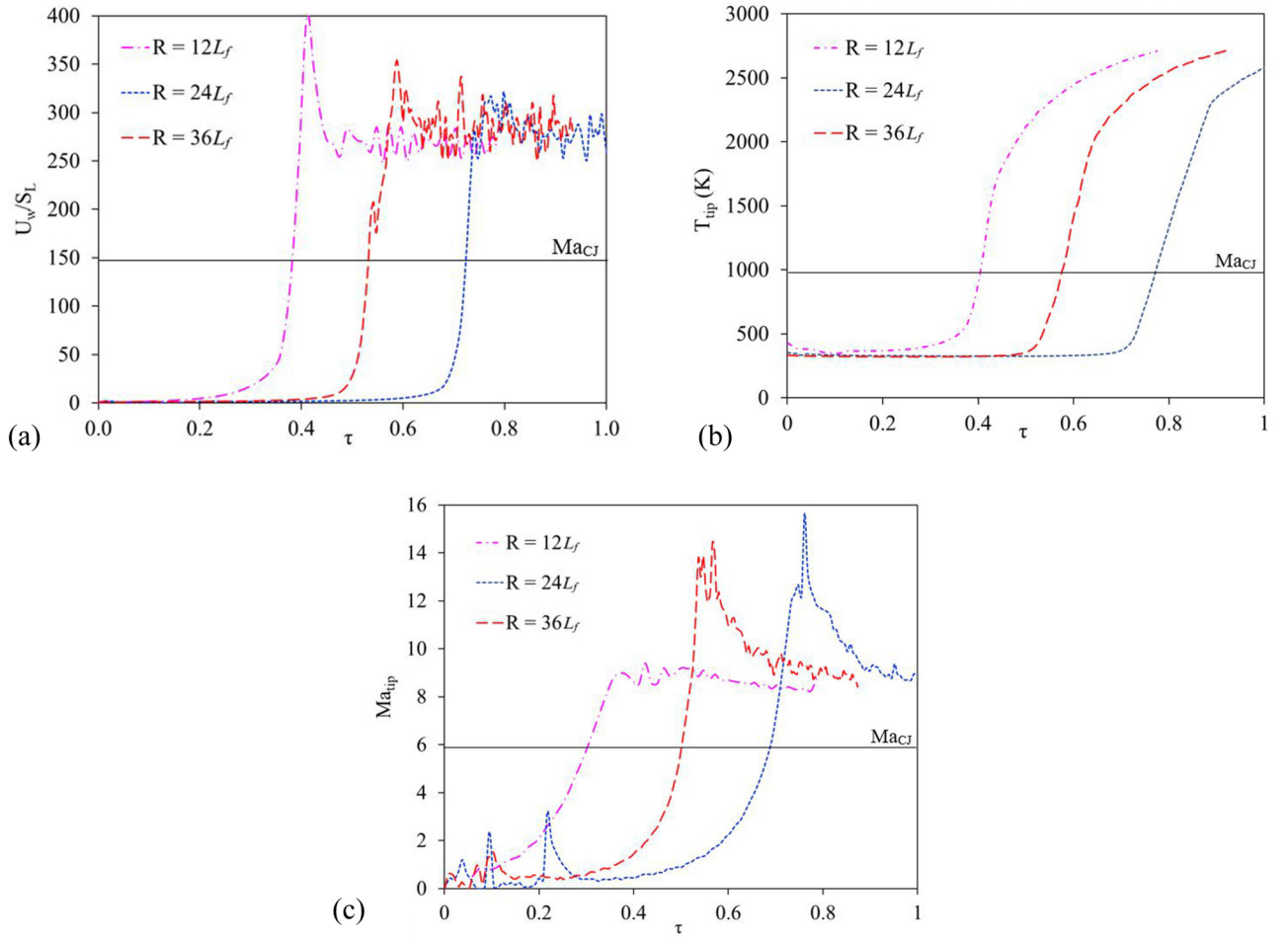

FIG. 12. The scaled burning rate U_w/S_L (a), the fuel temperature at the flame tip $T_{\rm tip}$ (b), and the flame tip Mach number $\mathrm{Ma}_{\rm tip}$ (c) vs the scaled time tS_L/R for the Le = 0.3, $\Theta = 8$ flames propagating in the obstructed channels with $\alpha = 2/3$, $\Delta Z = R/4$, and various $R/L_f = 12,\ 24,\ 36$.

For $k = C_p/C_v = 1.4$ and $\Theta = 8$ employed here, Eq. (11) yields $\mathrm{Ma}_{CJ} = 5.96$, which means that we deal with a detonation at the latest stages of burning in Fig. 12, above this horizontal line. After an abrupt onset of the detonation, the detonation velocity subsequently diminishes such that $\mathrm{Ma}_{\rm tip}$ saturates to a near steady value of $\mathrm{Ma}_{\rm tip} \approx 8.5$—almost the same for all three channel widths considered. While this saturation $\mathrm{Ma}_{\rm tip}$ exceeds Ma_{CJ}, such a deviation is acceptable, accounting for the fact that the estimation (11) is for a steady, one-dimensional (1D) detonation, while in the present work we deal with a multidimensional combustion front, whose tip velocity generally exceeds the total burning velocity (averaged over the entire flame front).

IV. CONCLUSION

In this work, we have investigated the effects of fuel mixture nonequidiffusivity (heat and mass imbalance, Le $\neq 1$) on flame propagation in obstructed channels with both open, nonreflecting ends by means of computational simulations of the hydrodynamic and combustion equations, including transport processes and chemical kinetics imitated by the first-order, one-step Arrhenius reaction. The interplays of the Lewis number Le with other geometrical parameters such as the channel width, the blockage ratio, and the obstacle spacing were also scrutinized. The flames are observed to undergo either oscillations, or acceleration, or a combination of both regimes. The Lewis number was found to have both quantitative and qualitative impacts on flame propagation, as there are transitions from the oscillations to acceleration, and vice versa, as Le changes. In cases, where oscillations were experienced for all Le considered (namely, at the thermal expansion ratio $\Theta = 8$, the blockage ratio $\alpha = 1/3$, the channel half-width $R = 12\ L_f$, and the obstacle spacing $\Delta Z = R/4$), the oscillation frequency decreased while the oscillation amplitude increased with Le. The flame experiences various propagation regimes: near steady oscillations, sudden acceleration, oscillations around a saturation velocity, or propagation at a constant velocity—depending on the impact of Le, independently, or because of its interplay with other parameters. The Le < 1 flames show a higher tendency of experiencing the sequence of initial near-steady flame propagation–sudden acceleration–oscillations around a saturation velocity, while the flame oscillations are encountered more in the cases of Le > 1.

The time of quasisteady flame propagation in the case of Le < 1 is found to be affected by the changes in the channel geometry parameters. Whether a flame oscillates or accelerates seems to be determined by the ratio of two competing forces: one from the expanding burnt gas, and the other from the viscous effect due to the fuel mixture ahead of the flame front. The Lewis number is found to contribute, significantly, to the magnitude of the push force and the flame response to the stretch caused by the hydraulic resistance, and thus, the dynamics and morphology of the flame front as it propagates. At the early stage of burning, compressibility is not significant; therefore, the flame oscillates. However, as $\mathrm{Ma}_{\mathrm{tip}}$ subsequently grows, accompanied by an increased fuel temperature, hot spots are formed ahead of the flame front. An interplay of the thermal explosion caused by flow compression and delayed burning in the pockets between the obstacles is found to be responsible for the sudden transition from the flame oscillations to acceleration.

ACKNOWLEDGMENTS

The study at West Virginia University was sponsored by the US National Science Foundation (NSF) through the CAREER Award No. 1554254 (V.A.) as well as by the West Virginia Higher Education Policy Commission through Grant No. HEPC.dsr.18.7 (V.A.). D.V. was supported by the National Science Foundation of China (NSFC) through Grant No. 52176118.

TABLE I. The resolution test.

	$\Delta Z_f/L_f$	U_w/S_L	$\lvert\Delta U_w/S_L\rvert$	Z_{tip}/R	$\lvert\Delta Z_{\mathrm{tip}}/R\rvert$
Le $= 0.3$	0.4	1.4499	–	2.5958	–
	0.2	1.9607	0.5108	2.5583	0.0375
	0.1	1.9751	0.0144	2.5542	0.0041
Le $= 1.0$	0.4	0.9126	–	2.5708	–
	0.2	2.0127	1.1001	2.5083	0.0625
	0.1	2.0186	0.0059	2.5125	0.0042
Le $= 2.0$	0.4	0.9828	–	2.5667	–
	0.2	1.7578	0.7750	2.5500	0.0167
	0.1	1.7447	0.0131	2.5500	0.0000

APPENDIX: RESOLUTION TEST

We performed the validation of the adaptive mesh size by monitoring the essential properties of the flames with the thermal expansion ratio $\Theta = 8$ and the Lewis numbers Le $=$ 0.3, 1, and 2, propagating in a channel of half-width $R/L_f =$ 24, blockage ratio $\alpha = 1/2$, and obstacle spacing $\Delta Z/R =$ 1/4. The mesh sizes in the range $0.1L_f \leqslant \Delta Z_f \leqslant 0.4L_f$ are tested to check the stability of the solution and whether the flames are sufficiently resolved. The values of the scaled burning rate U_w/S_L and the scaled flame tip position Z_{tip}/R for $\tau = 0.065$ are presented in Table I for the flames with

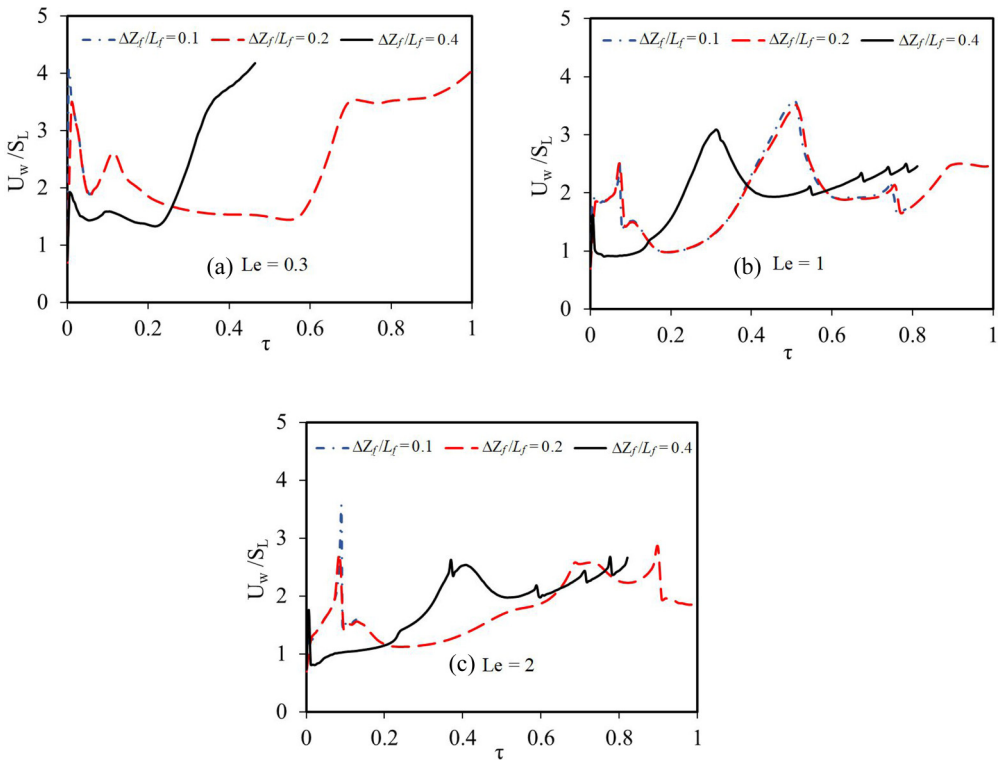

FIG. 13. The resolution test: the scaled burning rate U_w/S_L vs the scaled time tS_L/R for the thermal expansion ratio $\Theta = 8$, the half-width of the channel $R = 24\ L_f$, the blockage ratio $\alpha = 1/2$, the obstacle spacing $\Delta Z = R/4$, for various Lewis numbers Le $= 0.3$ (a), 1 (b), and 2 (c), and various mesh sizes $\Delta Z_f = 0.1\ L_f$ (dashed-dotted), $\Delta Z_f = 0.2\ L_f$ (dashed), and $\Delta Z_f = 0.4\ L_f$ (solid) in each panel.

$0.3 \leqslant \mathrm{Le} \leqslant 2.0$, and the mesh sizes of $\Delta Z_f = 0.1L_f, 0.2L_f, 0.4L_f$.

Figures 13(a)–13(c) show the plot of the scaled burning rate U_w/S_L vs the scaled time $\tau = tS_L/R$ for flames with $\mathrm{Le} = 0.3$, 1, and 2, respectively. A slight difference between the results obtained for resolutions of $\Delta Z_f = 0.2\ L_f$ and $0.1\ L_f$, as compared to a notable difference between the results obtained for $\Delta Z_f = 0.4\ L_f$ and $0.2\ L_f$, indicates convergence of the solution as the mesh size decreases. To be more rigorous, however, we might need to perform the following analysis. According to [26], the order of convergence supposedly correlates with the order of the truncation rate decay

$$\check{p} = \ln\left|\frac{\check{U}_3 - \check{U}_2}{\check{U}_2 - \check{U}_1}\right| / \ln(\check{r}), \tag{A1}$$

where $\check{U}_1$, $\check{U}_2$, and $\check{U}_3$ are the solutions provided by the coarse, medium and fine grids, respectively, and $\check{r} = \Delta z_{f,2}/\Delta z_{f,1} = \Delta z_{f,3}/\Delta z_{f,2}$ is the (constant) refinement ratio. In particular, the quantities of Z_{tip} for $\Delta z_f = 0.4, 0.2, 0.1$ in Table I yield $\check{p} \approx 3.2$ for $\mathrm{Le} = 0.3$ and $\check{p} = 3.9$ for $\mathrm{Le} = 1$. These estimations generally correlate with the overall order of approximation, which is between 2 and 4, being 2 for convective terms and 4 for diffusive terms.

[1] D. Valiev, V. Bychkov, V. Akkerman, C. K. Law, and L.-E. Eriksson, Flame acceleration in channels with obstacles in the deflagration-to-detonation transition, Combust. Flame **157**, 1012 (2010).

[2] G. Ciccarelli and S. Dorofeev, Flame acceleration and transition to detonations in ducts, Prog. Energy Combust. Sci. **34**, 499 (2008).

[3] S. Demir, V. Bychkov, S. H. R. Chalagalla, and V. Akkerman, Towards a predictive scenario of a burning accident in a mining passage, Combust. Theory Model. **21**, 997 (2017).

[4] Y. Z. Li and H. Ingason, Overview of research on fire safety in underground road and railway tunnels, Tunn. Undergr. Sp. Technol. **81**, 568 (2018).

[5] M. Silvestrini, B. Genova, G. Parisi, and F. J. Leon Trujillo, Flame acceleration and DDT run-up distance for smooth and obstacles filled tubes, J. Loss Prev. Process Ind. **21**, 555 (2008).

[6] V. Byckov, V. Akkerman, G. Fru, A. Petchenko, and L.-E. Eriksson, Flame acceleration in the early stages of burning in tubes, Combust. Flame **150**, 263 (2007).

[7] A. Adebiyi, R. Alkandari, D. Valiev, and V. Akkerman, Effect of surface friction on ultrafast flame acceleration in obstructed cylindrical pipes, AIP Adv. **9**, 035249 (2019).

[8] V. Akkerman, V. Bychkov, A. Petchenko, and L.-E. Eriksson, Flame oscillations in tubes with nonslip at the walls, Combust. Flame **145**, 675 (2006).

[9] A. DiStazio, C. Chauveau, G. Dayma, and P. Dagaut, Oscillating flames in micro-combustion, Combust. Flame **167**, 392 (2016).

[10] V. Bychkov, D. Valiev, and L.-E. Eriksson, Physical Mechanism of Ultrafast Flame Acceleration, Phys. Rev. Lett. **101**, 164501 (2008).

[11] V. N. Gamezo, T. Ogawa, and E. S. Oran, Flame acceleration and DDT in channels with obstacles: Effect of obstacle spacing, Combust. Flame **155**, 302 (2008).

[12] V. Bychkov, J. Sadek, and V. Akkerman, Analysis of flame acceleration in open or vented obstructed pipes, Phys. Rev. E **95**, 013111 (2017).

[13] A. Adebiyi, E. Ridgeway, R. Alkandari, A. Cathreno, D. Valiev, and V. Akkerman, Premixed flame oscillations in obstructed channels with both ends open, Proc. Combust. Inst. **37**, 1919 (2019).

[14] J. Yanez, M. Kuznetsov, and V. Bykov, Sudden acceleration of flames in open channels driven by hydraullic resistance, The 24th ICDERS, Taipei, Taiwan, 2013, p. 164.

[15] A. J. Aspden, M. S. Day, and J. B. Bell, Characterization of low Lewis number flames, Proc. Combust. Inst. **33**, 1463 (2011).

[16] S. D. Salusbury and J. M. Bergthorson, Maximum stretched flame speeds of laminar premixed counter-flow flames at variable Lewis number, Combust. Flame **162**, 3324 (2015).

[17] A. Adebiyi, O. Abidakun, G. Idowu, D. Valiev, and V. Akkerman, Analysis of non-equidiffusive premixed flames in obstructed channels, Phys. Rev. Fluids **4**, 063201 (2019).

[18] M. Alkhabbaz, O. Abidakun, D. Valiev, and V. Akkerman, Impact of the Lewis number on flame acceleration at the early stage of burning in pipes, Phys. Fluids **31**, 083606 (2019).

[19] S. Bilgili, V. Bychkov, and V. Akkerman, Impacts of the Lewis and Markstein numbers on premixed flame acceleration in channels due to wall friction, Phys. Fluids **34**, 013604 (2022).

[20] N. Chakraborty and R. S. Cant, Effects of Lewis number on turbulent scalar transport and its modelling in turbulent premixed flames, Combust. Flame **156**, 1427 (2009).

[21] O. Abidakun, A. Adebiyi, D. Valiev, and V. Akkerman, Impacts of fuel nonequidiffusivity on premixed flame propagation in channels with open ends, Phys. Fluids **33**, 013604 (2021).

[22] A. Petchenko, V. Bychkov, V. Akkerman, and L.-E. Eriksson, Flame-sound interaction in tubes with nonslip walls, Combust. Flame **149**, 418 (2007).

[23] O. J. Ugarte, V. Bychkov, J. Sadek, D. Valiev, and V. Akkerman, Critical role of blockage ratio for flame acceleration in channels with tightly spaced obstacles, Phys. Fluids **28**, 093602 (2016).

[24] V. Bychkov, V. Akkerman, D. Valiev, and C. K. Law, Influence of gas compression on flame acceleration in channels with obstacles, Combust. Flame **157**, 2008 (2010).

[25] R. Chue, J. Clarke, and J. H. Lee, Chapman-Jouguet deflagrations, Proc. Roy. Soc. Lond. A **441**, pp. 607 (1993).

[26] H. Versteeg and W. Malalasekera, *An Introduction to Computational Fluid Dynamics. The Finite Volume Method*, 2nd ed. (Pearson Education, Prentice Hall, New York, 2007).